

Reproducibility of graph metrics of human brain structural networks

Jeffrey T. Duda^{1,*}, Philip A. Cook¹ and James C. Gee¹

¹ Penn Image Computing and Science Laboratory, University of Pennsylvania, Department of Radiology, Philadelphia, PA, USA

Correspondence*:

Jeffrey T. Duda

Penn Image Computing and Science Laboratory, University of Pennsylvania, Department of Radiology, 3600 Market Street, Suite 370, Philadelphia, PA, USA, jtduda@seas.upenn.edu

Neuroinformatics with the Insight ToolKit

2 ABSTRACT

Recent interest in human brain connectivity has led to the application of graph theoretical analysis to human brain structural networks, in particular white matter connectivity inferred from diffusion imaging and fiber tractography. While these methods have been used to study a variety of patient populations, there has been less examination of the reproducibility of these methods. A number of tractography algorithms exist and many of these are known to be sensitive to user-selected parameters. The methods used to derive a connectivity matrix from fiber tractography output may also influence the resulting graph metrics. Here we examine how these algorithm and parameter choices influence the reproducibility of proposed graph metrics on a publicly available test-retest dataset consisting of 21 healthy adults. The dice coefficient is used to examine topological similarity of constant density subgraphs both within and between subjects. Seven graph metrics are examined here: mean clustering coefficient, characteristic path length, largest connected component size, assortativity, global efficiency, local efficiency, and rich club coefficient. These reproducibility of these network summary measures is examined using the intraclass correlation coefficient (ICC). Graph curves are created by treating the graph metrics as functions of a parameter such as graph density. Functional data analysis techniques are used to examine differences in graph measures that result from the choice of fiber tracking algorithm. The graph metrics consistently showed good levels of reproducibility as measured with ICC, with the exception of some instability at low graph density levels. The global and local efficiency measures were the most robust to the choice of fiber tracking algorithm.

22 **Keywords:** Structure, Tractography, Connectivity, Brain, Network, Reproducibility, Graph

1 INTRODUCTION

Combining magnetic resonance imaging (MRI) of the human brain with graph theory analysis has emerged as a powerful approach to studying large-scale networks of both structural and functional connectivity. In the case of structural connectivity, the use of diffusion weighted MRI and associated white matter fiber tractography methods provide the ability to identify the long-range pathways that connect cortical regions and form a network architecture (Basser et al., 2000; Lazar et al., 2003; Hagmann et al., 2003; Xue et al., 1999). The use of graph theoretical analysis to study the topology and structure of these large scale networks is an increasingly active topic of research (Hagmann et al., 2008; Zalesky et al., 2010; Cheng et al., 2012a; Bastiani et al., 2012; Irimia and Van Horn, 2012; Sporns, 2011; Fornito et al., 2012). These methods have been used to examine the structural consequences of neurological disorders (Xie and

32 He, 2012; Guye et al., 2010; Martin, 2012) as well as the relationship between structure and function
33 (Hagmann et al., 2008; Honey et al., 2009, 2007).

34 Previous studies examining the reproducibly of graph-based metrics in functional networks have shown
35 good levels of reproducibly in MEG (Deuker et al., 2009), fMRI using BOLD contrast (Telesford et al.,
36 2010; Braun et al., 2012; Schwarz and McGonigle, 2011; Liang et al., 2012; Weber et al., 2013) and arte-
37 rial spin labeling (Weber et al., 2013). A number of studies have also examined reproducibly in structural
38 networks, each focusing on various aspects of the complex processing pipeline that is a prerequisite for
39 these measures. These have included studies of diffusion spectrum imaging (Cammoun et al., 2012; Bas-
40 sett et al., 2011) and high angular resolution diffusion imaging (Dennis et al., 2012). Some studies have
41 examined probabilistic tractography (Owen et al., 2013; Vaessen et al., 2010). Diffusion tensor imaging
42 (DTI) based studies using deterministic tractography have included the examination of tractography seed
43 density (Cheng et al., 2012b), anatomic label density (Bassett et al., 2011), and studies examining a va-
44 riety of network measures (Cheng et al., 2012b; Irimia and Van Horn, 2012). Further exploration of the
45 reproducibility of these graph metrics as it relates to their utility in longitudinal studies (Telesford et al.,
46 2013).

47 In the paper we constrain our analysis to DTI-based deterministic fiber tractography. Within this con-
48 straint, we examine multiple algorithms for computing streamlines to examine their influence on the final
49 graph metrics. A set of manually defined cortical parcellations (Klein and Tourville, 2012) is used along
50 with a more common template-based parcellation scheme (Tzourio-Mazoyer et al., 2002). The intraclass
51 correlation coefficient (ICC) is used to examine the reproducibility of network summary measures that re-
52 sults from combinations of fiber tracking algorithm and anatomical label set. The dice coefficient provides
53 a measure of topographical similarity to examine the reproducibility of subgraphs extracted as a function
54 of graph density. Graph curves are constructed for a variety of metrics and functional data analysis is used
55 to examine how these metrics differ as a function of graph density or other parameters that are specific
56 to a given metric. We use freely available data and software to create a framework that facilitates future
57 extensions that may examine additional aspects of the processing as well as the comparison to, or addition
58 of, multiple imaging modalities.

2 MATERIALS & METHODS

2.1 NEUROIMAGING DATA

59 The Multi-Modal MRI Reproducibility Resource (Landman et al., 2011), informally known as the Kirby
60 dataset (<http://www.nitrc.org/projects/multimodal>), provides a publicly available test-
61 retest data set consisting of 21 healthy control subjects (11 males). The mean age is 31.76 ± 9.35 with a
62 range of [22,61]. This data set provides a multitude of MR image types, but here only the T1-weighted
63 anatomical images and diffusion tensor images are examined. The T1 images have a resolution of $1.2 \times$
64 $1.0 \times 1.0\text{mm}$. The distributed diffusion images have a resolution of $0.828125 \times 0.828125 \times 2.2\text{mm}$. The
65 diffusion data includes a single $b = 0$ volume and 34 directional diffusion weighted images acquired with
66 $b = 700\text{s/mm}^2$.

2.2 ANATOMICAL LABELING

67 A graph consists of nodes and the edges that connect those nodes. To construct a graph from a brain, a set
68 of anatomical labels are used to define the nodes of the graph. To determine if manually defined cortical
69 labels would provide an inherent advantage in reproducibility we used of the Mindboggle dataset which
70 provides a set of manually drawn cortical regions (DKT31) along with a skull-stripped image for a single
71 time point for each subject in the Kirby data set (Klein and Tourville, 2012). To utilize these labels in
72 network creation we performed an intra subject registration between each subject's two T1 images. A
73 brain mask was created from the provided skull-stripped T1 image by thresholding and a morphological
74 closing. This mask was warped into the unlabeled T1 image space and used to create a skull-stripped
75 image. For each time, a transformation was found between the skull-stripped T1 image and the $b=0$ image,
76 acquired as part of the DTI acquisition. In all subjects, the manually defined labels were propagated into
77 the DTI space for both time points using the appropriate composed transform.

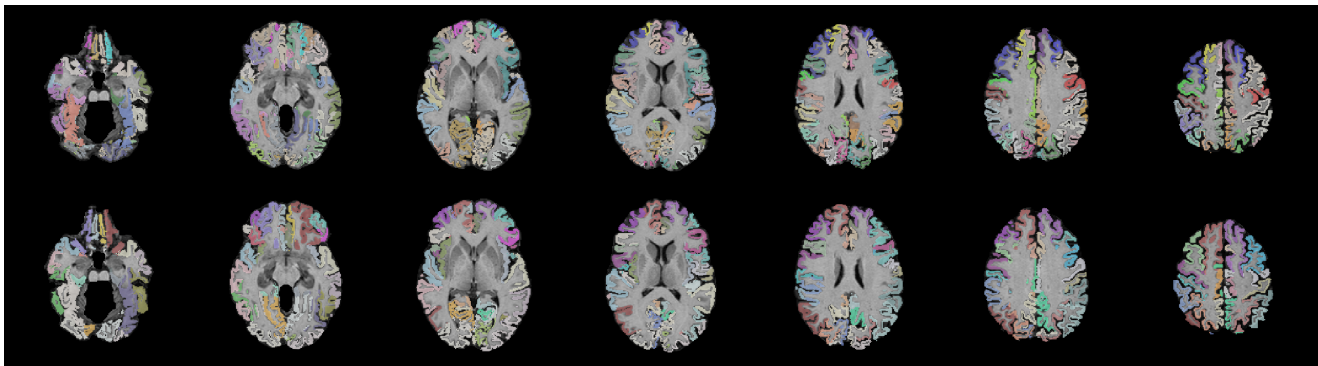


Figure 1. Two sets of anatomical labels are used to define the networks. The template based AAL labels (top) and The DKT31 manually defied labels that are provided via Mindboggle (bottom). The AAL labels have been masked to only include gray matter

78 One of the most common label sets used in studies of both functional and structural con-
 79 nectivity is the AAL label set (Tzourio-Mazoyer et al., 2002) which is a template based la-
 80 bel set. An existing multivariate template had been created from the Kirby dataset using the
 81 `antsMultivariateTemplateConstruction.sh` tool, part of the Advanced Normalization
 82 Tools (ANTs) software package (Avants et al., 2009). The `antsRegistration` tool was used to find
 83 a deformable mapping between the T1 template image distributed with the AAL label and the popula-
 84 tion specific template created from the Kirby data. In order to transform these labels into each subject's
 85 DTI space, it was necessary to find a transform from the template to each subject's T1 and from T1
 86 to DTI within each subject. For the template-to-T1 transform, the `antsCorticalThickness.sh`
 87 tool was used. This software first applied a bias correction using the N4 algorithm (Tustison et al.,
 88 2010). Next a registration based skull stripping was performed to provide a cerebrum mask of the T1
 89 image. This was followed by a final cerebrum-only registration to the template. These transforms were
 90 composed with the T1-to-DTI transforms, providing a single transform that was used to warp the the
 91 AAL labels into DTI space using nearest neighbor interpolation. Labels of structures outside of the
 92 cerebrum were removed. Many AAL labels include both gray and white matter, here the labels were
 93 masked to only include voxels that were identified as cortical gray matter by the DKT31 labels described
 94 in the previous section. The AAL labels for deep gray structures (e.g. thalamus) were not masked but
 95 used in their entirety. Both label sets are illustrated in figure 1, while the entire processing scheme
 96 is illustrated in figure 2. The availability of the processing scripts is intended to provide a framework
 97 that allows for convenient exploration of alternate anatomical labels, such as the anatomical parcel-
 98 lations that may be obtained via FreeSurfer (<http://surfer.nmr.mgh.harvard.edu>) or the
 99 UCLA Multimodal Connectivity Package ([http://ccn.ucla.edu/wiki/index.php/UCLA_](http://ccn.ucla.edu/wiki/index.php/UCLA_Multimodal_Connectivity_Package)
 100 [Multimodal_Connectivity_Package](#)), both of which have been used in previous graph-theory
 101 based examinations of structural connectivity based on diffusion-weighted imaging.

2.3 DIFFUSION DATA PREPROCESSING

102 The Camino toolkit (Cook et al., 2006) was used to calculate diffusion tensor images via a weighted linear
 103 fitting (Basser et al., 1994; Salvador et al., 2005), and was used for subsequent deterministic tractography.
 104 The brain masks defined in T1 space were warped into DTI space and used to prevent tracking outside
 105 the brain. Fractional anisotropy (FA) images were calculated and a tractography seed-map was created to
 106 include all voxels in the cerebrum with an FA of at least 0.2.

107 One of the primary differences among the various approaches to deterministic tractography is the al-
 108 gorithm used to determine the direction that a streamline should proceed from a given point. Here we
 109 examine four different approaches:

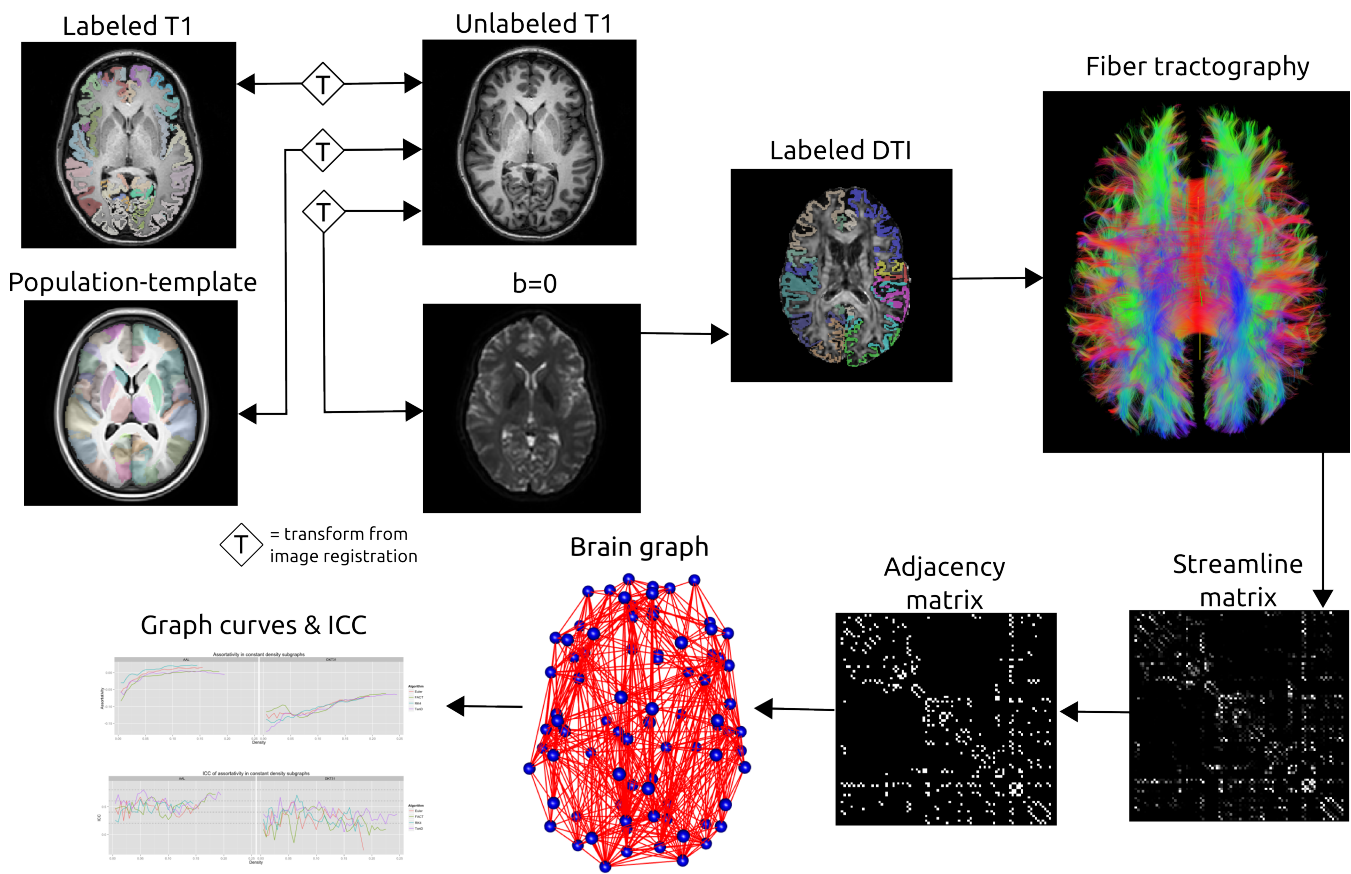


Figure 2. Schematic of the network processing scheme. Image registration is used to find transformations between the T1 image and: the T1 image for that subject's other time point; the population template; the b=0 image acquired as part of the DTI acquisition. Labels are transformed into the DTI space where fiber tractography is performed. A matrix is created that records the number of streamline connecting each pair of labeled regions. This matrix is thresholded as constant density to create an adjacency matrix which defines connections in a brain graph. Graph curves are generate by calculating network summary measures over a range of density values and ICC plots are used to examine the reproducibility of the metrics.

- 110 1. Fiber Assignment by Continuous Tracking (FACT) - The primary direction of diffusion (PDD) is
111 followed until the streamline enters a new voxel (Xue et al., 1999).
- 112 2. Euler - The PDD is followed for a constant step size (Basser et al., 2000).
- 113 3. Rourth-order Runge-Kutta (RK4) - The direction of the step is determined by taking and averaging a
114 weighted series of partial steps (Basser et al., 2000).
- 115 4. Tensor Deflection (TEND) - The local fiber trajectory is a function of the previous direction and the
116 local diffusion tensor (Lazar et al., 2003)
- 117 Shared parameters used in the fiber tracking were held constant as follows
- 118 1. Streamlines were terminated if curvature of more than 90 degrees over 5 steps was detected.
119 2. Streamlines were terminated if an FA value of less of 0.2 was encountered.
120 3. A step size of 0.5mm was used.
121 4. Linear interpolation of the primary direction of diffusion was used for Euler and RK4.

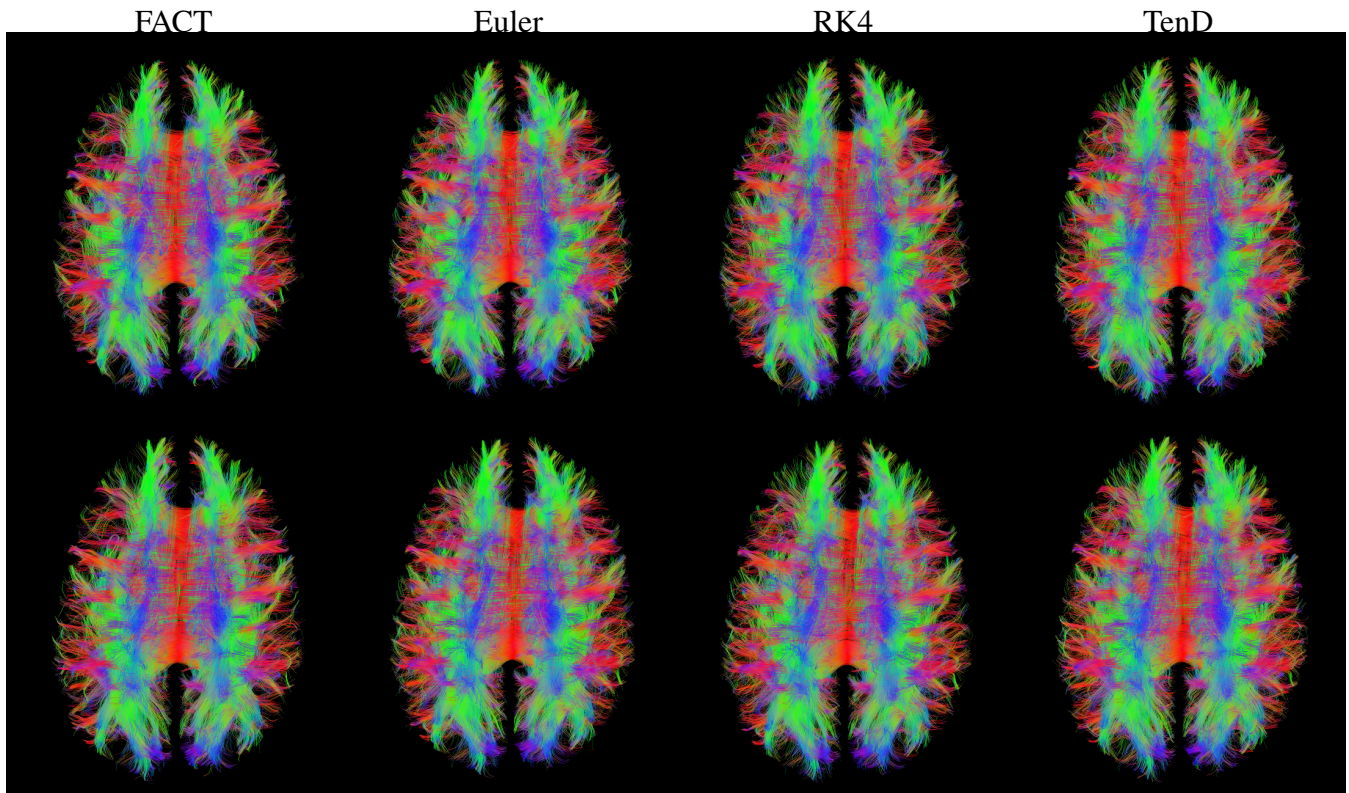


Figure 3. Fiber tracts generated using each method are illustrated for both time points in a single subjects. For visualization, tract sets are sampled to display 5% of the tracts at 25% opacity. Tract points are colored to illustrate local streamline direction.

122 Figure 3 illustrates the fiber tracts for all methods for a single subject. The script used to generate
 123 these streamlines, `deterministic_mmrr21.pl`, is available as part of the git repository that con-
 124 tains all of the processing scripts for the work presented here (<https://github.com/jeffduda/StructConnRepro>). Relatively small changes to this script would allow users to explore additional
 125 deterministic tractography methods as well as probabilistic methods which are also available in the Camino
 126 toolkit.
 127

2.4 GRAPH GENERATION

128 While the nodes of a graph were defined using anatomical labels, the edges of the graph were defined
 129 by using fiber tractography to identify white matter pathways that connect brain regions. For a given set
 130 of streamlines, the `connmat` tool provided by the Camino toolkit was used to generate a connectivity
 131 matrix that records how many streamlines connect each pair of regions in a given set of target regions.
 132 This program starts at the seed point for a streamline and proceeds outward in each direction to determine
 133 the two target regions encountered. Only streamlines that connect two unique regions are retained and a
 134 given streamline may be only be counted as connecting a single pair of target regions. Fiber tractography
 135 does not provide a measure of directionality (i.e. neither node can be considered a starting point or ending
 136 point) so the resulting matrices resulting in undirected graphs.

Graphs are often compared by first ensuring that they have the same density (Achard et al., 2006; Bassett et al., 2006), where density for an undirected graph is defined as:

$$D(G) = \frac{\|E(G)\|}{(\|N(G)\|(\|N(G)\| - 1))}$$

137 where $N(G)$ is the set of all nodes in graph G and $E(G)$ is the set of all edges in G . The number of
 138 nodes in the graph and the desired density determine the number of edges that the graph should contain.
 139 Edges of higher weights are given priority and lower weighted edges are removed to obtain the desired
 140 density level. The weights of the remaining edges are then set to 1 for a final binarized graph. This
 141 cumulative thresholding provides a normalized method for comparing network measures as it results
 142 in the comparison of graphs with an equal percentage of significant connections. Graphs are typically
 143 compared over a range of density levels. Here, we only directly compare measures obtained from graphs
 144 with an equal number of nodes and thus an equal number of edges after density thresholding.

2.5 NETWORK METRICS

145 A large number of graph metrics are available for quantifying properties of binary, undirected networks
 146 (Rubinov and Sporns, 2010). Here we examine a number that are common in current literature: largest
 147 connected component size (Bassett et al., 2011), assortativity (Newman, 2006; Bassett et al., 2008), clus-
 148 tering coefficient (Watts and Strogatz, 1998), characteristic path length (Watts and Strogatz, 1998), global
 149 and local efficiency (Latora and Marchiori, 2001), and rich club coefficient (Collin et al., 2013). An
 150 ITK module named Petiole (<https://github.com/jeffduda/Petiole>) was created to calcu-
 151 late these network measures from 2D connectivity matrices. This module incorporates and extends an
 152 existing implementation of a graph class (Tustison et al., 2008) and provides ITK functions for a variety
 153 of graph metrics while using the matlab-based Brain Connectivity Toolkit (Rubinov and Sporns, 2010) for
 154 algorithmic guidance. While many of these metrics include implementations for weighted graphs and/or
 155 directed graphs, here we focus on their application to unweighted, undirected graphs. Summaries and
 156 equations for these metrics are provided here:

157 *Size of Largest Connected Component.* A connected component of a graph is a subset of the graph, G_i ,
 158 where there exists a path between all pairs of nodes and for which no path exist to additional nodes in
 159 G . The largest connected component is the G_i with the greatest number of nodes, $\|N(G_i)\|$. This measure
 160 relates to the global level of connectivity within a subject's brain network Bassett et al. (2011).

Assortativity. The degree of a node is the number of neighboring nodes that it connects to (i.e. shares
 an edge with). Assortativity measures how preferentially nodes of similar degree connect to one another
 (Newman, 2006) and is defined as:

$$A = \frac{\frac{1}{E} \sum_i j_i k_i - [\frac{1}{E} \sum_i \frac{1}{2}(j_i + k_i)]^2}{\frac{1}{E} \sum_i \frac{1}{2}(j_i^2 + k_i^2) - [\frac{1}{E} \sum_i \frac{1}{2}(j_i + k_i)]^2}$$

161 where j_i, k_i are the degrees of the nodes connected by edge i and $E = \|E(G)\|$. High assortativity
 162 suggests higher network resilience, making a network less vulnerable to attack (Newman, 2002).

Clustering Coefficient. This measure quantifies how likely is that two nodes with a common neighbor
 are connected to one another (Watts and Strogatz, 1998). Here we calculate the clustering coefficient at
 each node and calculate the mean over all nodes in the network for our final network summary measure.
 The clustering coefficient at node i is given by:

$$C_i = \frac{e_i}{\|K_i\|(\|K_i\| - 1)}$$

163 where K_i is the set of all nodes that share an edge with i and e_i is the set of all edges that connect nodes
 164 in K_i .

Characteristic Path Length. The pathlength, L_{ij} , that connects two nodes, i and j , is defined as the
 minimum number of edges that must be traversed to travel from i to j (Dijkstra, 1959). The characteristic
 path length is the average pathlength over all possible pairs of connections in a graph. In an undirected
 graph this is:

$$L = \frac{1}{\|N(G)\|(\|N(G)\| - 1)} \sum_{ij \in G, i \neq j} L_{ij}$$

165 This measure is only defined for fully connected graphs. Here, we apply the density thresholding first and
 166 then extract the largest connected component in order to calculate the characteristic path length.

Global Efficiency. This measure is related to the characteristic path length, in that it attempts to quantify the mean efficiency between any two nodes in the graph. Unlike the characteristic path length, this metric is defined for both connected and unconnected graphs (Latora and Marchiori, 2001).

$$F_{glob} = \frac{1}{\|N(G)\|(\|N(G)\| - 1)} \sum_{i \neq j \in G} 1/L_{ij}$$

Local Efficiency. This metric relates to fault tolerance and examines efficiency between neighbors on a node i , if that node were removed from the graph (Latora and Marchiori, 2001).

$$F_{loc} = \frac{1}{\|N(G)\|} \sum_{i \in n} F(G_i)$$

167 where G_i is the subgraph of G that results from removing node i .

Rich Club Coefficient This measures quantifies how preferentially the high-degree nodes (i.e. rich nodes) in a graph connect to other high-degree nodes (Colizza et al., 2006).

$$R(G, k) = \frac{\|E(G, k)\|}{\|N(G, k)\|(\|N(G, k)\| - 1)}$$

168 where $N(G, k)$ is the set of nodes of degree k or higher and $E(G, k)$ is the set of edges connecting two
169 nodes in $N(G, k)$.

2.6 GRAPH CURVES

170 The metrics listed above are all applied to thresholded binary graphs. As discussed earlier, this binary
171 graph result from thresholding at a constant density. These metrics may then be treated as functional
172 curves of metric vs. graph density. By doing this, we are able to compare binary graphs in a way that
173 incorporates the continuous structure of the original connectivity matrices. The rich club coefficient how-
174 ever is dependent upon two parameters, the graph density and, k , the degree threshold used to determined
175 what constitutes a rich-node. For this metric we threshold at the highest density common to all graphs
176 and explore how the value changes with k . For all other metrics, we examine their curves as a function of
177 graph density.

2.7 STATISTICAL ANALYSIS

Before examining how the graph metrics change with density it is necessary to examine the maximum density of the graphs to determine the range over which graphs may be compared. Additionally, it is interesting to examine the topological similarity in the thresholded graphs. This is done using the dice coefficient which measures similarity between two graphs as:

$$Dice(x, y) = \frac{2\|E(x) \cap E(y)\|}{\|E(x)\| + \|E(y)\|}$$

178 where edges are considered equal if they connect the same two nodes. This is equivalent to treating each
179 connectivity matrix as a binarized 2D image and using the Dice metric to measure overlap. The mean
180 intra- and inter-subject topological similarity was computed over a range of densities for each combination
181 of tracking algorithm and anatomical label sets. This allows us to examine the reproducibility of within-
182 subject topography compared to between subject topography. This metric is limited to lie in the range [0, 1]
183 and can be interpreted as a measure of degree of overlap between graphs. This provides a stricter metric
184 than measuring overlap between sets of nodes as complete node-overlap is a necessary but incomplete
185 condition for complete edge-overlap.

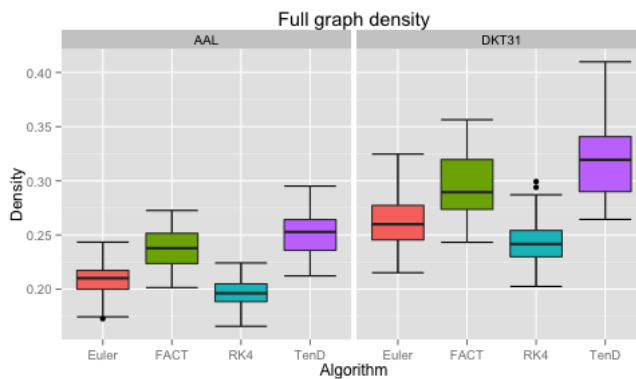


Figure 4. Boxplots illustrating the density values for unthresholded connectivity matrices for all subjects and all time points, grouped by fiber tracking algorithm (Euler,FACT,RK4,TEND) and anatomical label set (AAL,DKT31).

Graph curves are used to examine the reproducibility of the graph metrics as a function of an independent parameter, typically graph density. At each point along the curve, reproducibility of the metric is quantified using the ICC:

$$ICC = \frac{\sigma_{bs}^2}{\sigma_{bs}^2 + \sigma_{ws}^2}$$

where σ_{bs}^2 is the between-subject variance and σ_{ws}^2 is the within subject variance. The 'ICC' package for R is used for this calculation. The ICC is plotted along with the mean graph metrics for each combination of algorithm and label set. At points where little to no variance exists in a graph metric, the ICC is not calculated as it becomes unstable under those conditions. The following guidelines may be used to interpret ICC values: $ICC < 0.2$ 'poor agreement'; $0.21 - 0.40$ 'fair agreement'; $0.41-0.60$ moderate agreement; $0.61-0.80$ 'strong agreement'; $ICC > 0.8$ 'near perfect agreement' (Telesford et al., 2010; Montgomery et al., 2002). Dashed lines indicating the boundaries of these categories have been included on all ICC plots to aid interpretation.

To identify group differences that result from fiber tracking algorithm we incorporated methods from functional data analysis (FDA) which treats each curve as a function. For each group, the set of all curves were averaged to create a single mean curve. While there are a variety of methods for computing the difference between two curves, here we chose the simplest method, the non-parametric permutation test. Each mean curve was treated a function and the area between the group mean curves was found. Individual group assignments were then permuted using random sampling without replacement and then used to calculate mean curves. The area between the random-group mean curves was calculated. This was performed iteratively ($i=10000$). We recorded, x , the number of times area between the mean curves from the randomly assigned groups is larger than the area between the true group mean curves. The p-value for the true group difference is then defined as x/i . We report these differences for between-algorithm curves as they derive from graph of equal size, but do compare curves that derive from different anatomical label sets.

3 RESULTS

3.1 NETWORK DENSITY

Maximal densities for connectivity matrices across all tracking algorithm ranged from 0.17 to 0.30 for the AAL labels and from 0.20 to 0.41 for DKT31. Maximal densities in the DTK31 data was generally higher than in the AAL as illustrated in figure 4. Both label sets had the same lowest-to-highest ordering of mean maximal density within algorithms: $RK4 < Euler < FACT < TEND$.

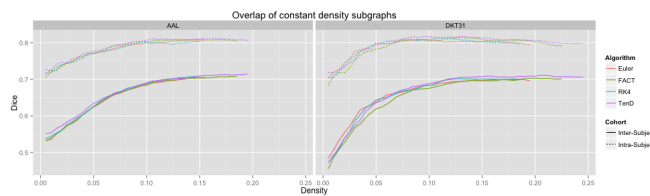


Figure 5. Connectivity matrices were thresholded over a range of density values. At each density level, consistency of network topography was estimated by calculating the mean dice overlap for both intra subject and intersubject pairs.

Table 1. Functional data analysis is used along with permutation testing to look for differences in dice overlap measures between graph generated from different fiber tracking algorithms. Upper triangular p-values are for the AAL labels, while lower triangular are for the DTK31 label set (* indicated significance).

	Intra Subject				Inter Subject			
	Euler	FACT	RK4	TEND	Euler	FACT	RK4	TEND
Euler		0.9555	0.9864	0.6549		0.7770	0.2675	0.0351*
FACT	0.4186		0.7970	0.9524	0.0002*		0.2586	0.0355*
RK4	0.8780	0.6179		0.5358	0.0632	0.0014*		0.1335
TEND	0.3952	0.6655	0.7564		0.0001*	0.0003*	0.0838	

3.2 NETWORK TOPOLOGY

Dice coefficients for intra-subject similarity ranged from 0.70 to 0.81 for the AAL labels and from 0.59 to 0.82 for the DTK31 labels. Inter-subject similarity ranged from 0.51 to 0.71 for AAL labels and from 0.32 to 0.71 for the DTK31 labels. For all algorithm-label pairings, intra-subject overlap was greater than inter-subject overlap across the range of densities as illustrated in figure 5. Permutation testing of intra-subject dice vs. density curves did not reveal any significant differences between algorithms for either label set. However, a number of differences were found in the inter-subject comparisons. The resulting p-values are listed in table 1.

3.3 NETWORK SUMMARY MEASURES OVER GRAPH DENSITY

For each combination of tracking and label set, the mean curves that were calculated to examine how the metrics change as a function of graph density are illustrated in figure 6 along with the ICC curves that quantify reproducibility. In some cases, ICC values may not be calculate due to insufficient variation in the metric. Only the characteristic path length curves exhibit a different shape between label sets, and only at low density values. This is likely a results of the smaller number of regions in DKT31 label set. Clustering coefficient, and global and local efficiency exhibit the most similarity across label sets. Comparing within metric and within label set, the fiber tracking algorithms appear consistent as far as shape. Functional data analysis, along with permutation testing does reveal a number of significant differences between graph curves however, as listed in table 2. No significant differences were found between tracking algorithms using the DKT31 labels. Within the AAL labels, significant differences were found between RK4 and TEND for four of the six metrics examined.

3.4 RICH CLUB COEFFICIENT OVER NODE-DEGREE

Because the rich club coefficient requires the selection of multiple parameters, we chose to examine how this metric changes as a function of k , the node degree that determines what is considered a 'rich'

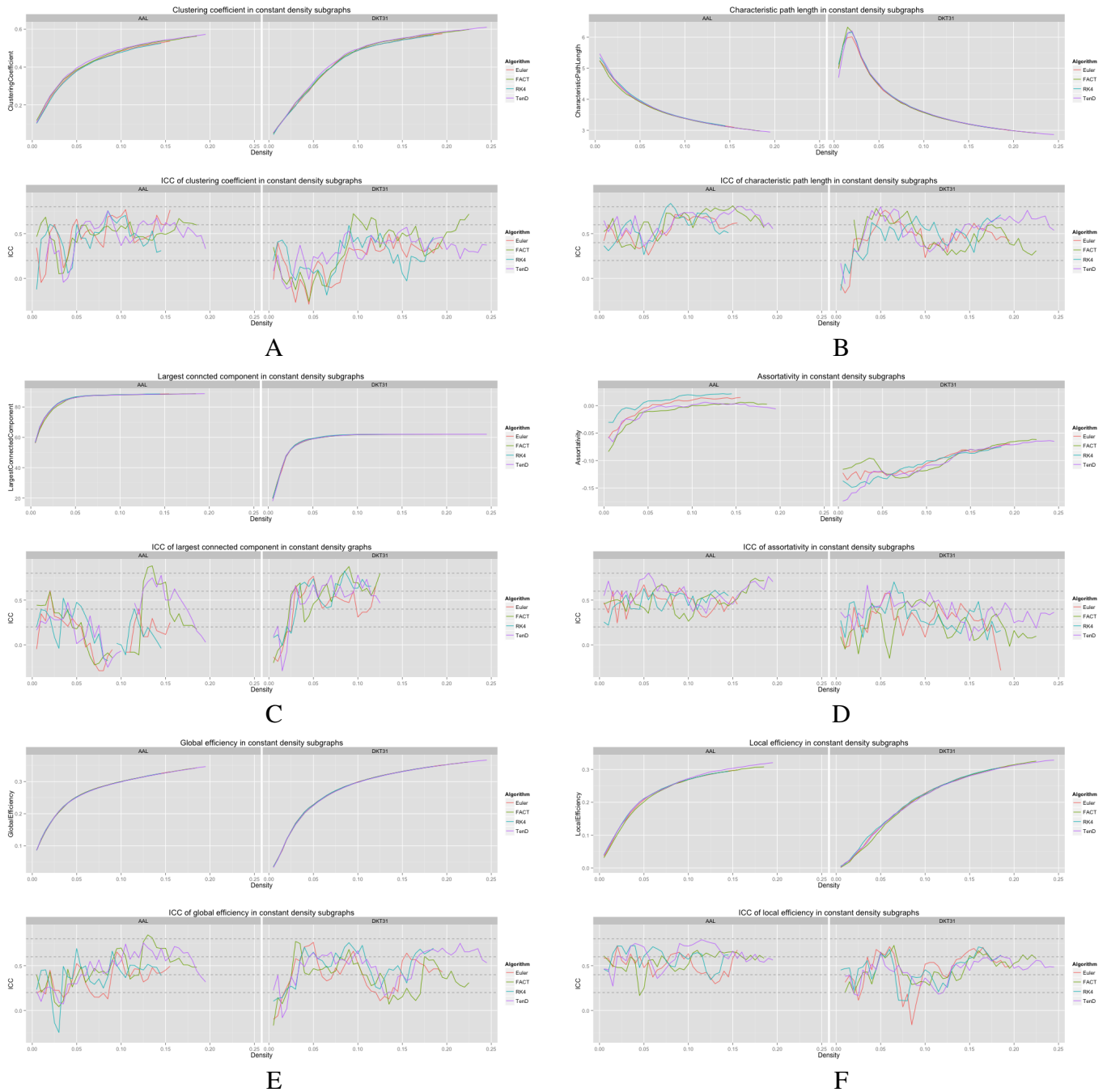


Figure 6. Graph metric vs. graph density plots along with corresponding ICC plots for A) Mean clustering coefficient B) Characteristic path length C) Largest connected component size D) Assortativity E) Global efficiency and F) Local efficiency

230 node. The plots for the mean graph curves and ICC coefficients are illustrated in figure 7. The results
 231 are similar to the examinations over graph density in that the same shape appears for both label sets, but
 232 with a scaling difference and the tracking algorithms have similar shapes but within the AAL networks,
 233 differences were found in the RK4-FACT ($p=0.0338$) and RK4-TEND ($p=0.0252$) comparisons. The
 234 p-values for all comparisons are listed in table 3

Table 2. Functional data analysis is used along with permutation testing to look for pair-wise differences in graph-metric vs. graph-density curves that result from different fiber tracking algorithms and label sets. Only the first time-point for each subject is used. For each metric, the upper-triangular values are for p-values for the AAL labels while the lower-triangular values were generated with the DKT31 label set (* indicated significance).

	Clustering Coefficient				Characteristic Path Length			
	Euler	FACT	RK4	TEND	Euler	FACT	RK4	TEND
Euler	0.2164	0.5296	0.0346*		0.2786	0.2389	0.4728	
FACT	0.6962		0.0246*	0.2822	0.9982		0.0145*	0.1235
RK4	0.9927	0.7958		0.0049*	0.8465	0.9199		0.3031
TEND	0.1327	0.8858	0.2061		0.4854	0.6459	0.8234	
	Connected Component Size				Assortativity			
Euler	0.3471	0.9324	0.7556		0.3680	0.3294	0.4651	
FACT	0.9447		0.0468*	0.3025	0.6361		0.0270*	0.8877
RK4	0.9998	0.7610		0.4748	0.9326	0.3250		0.0666
TEND	0.7912	0.8336	0.7269		0.8272	0.4021	0.9895	
	Global Efficiency				Local efficiency			
Euler	0.8617	0.9861	0.7272		0.4579	0.9227	0.6065	
FACT	0.8677		0.6882	0.7667	0.8794		0.2486	0.1230
RK4	0.6295	0.9415		0.8677	0.9745	0.4413		0.7557
TEND	0.9977	0.9633	0.7438		0.8752	0.7987	0.4775	
	Euler	FACT	RK4	TEND	Euler	FACT	RK4	TEND

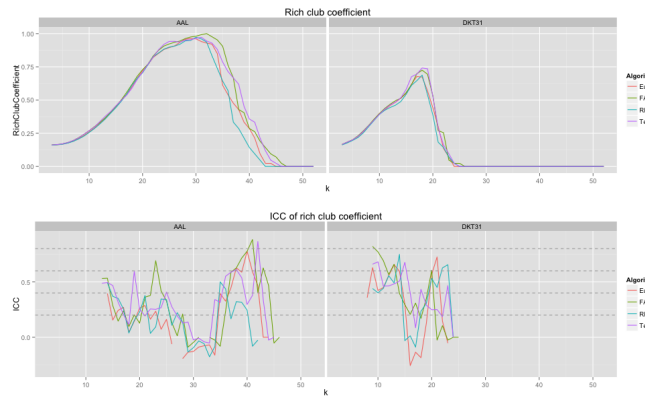


Figure 7. Rich club coefficient was examined over a range of levels, k , and a constant graph density of 0.15

4 DISCUSSION

4.1 NETWORK TOPOLOGY

235 Although a number of studies have examined the reproducibility of graph metrics on structural brain
 236 networks derived from DTI-based fiber tractography, there are no known papers that focus on the selec-
 237 tion of deterministic tracking algorithm. To facilitate later examination of graph metrics as a function of

Table 3. Functional data analysis is used along with permutation testing to look for differences in rich club coefficients generated from different fiber tracking algorithms. Upper triangular p-values are for the AAL labels, while lower triangular are for the DTK31 label set (* indicated significance).

	Euler	FACT	RK4	TEND
Euler		0.3359	0.6830	0.2064
FACT	0.8944		0.0338*	0.8537
RK4	0.9282	0.7219		0.0252*
TEND	0.7548	0.8800	0.3360	
	Euler	FACT	RK4	TEND

graph density, we first examined the reliability of identifying subgraphs by thresholding. Using the dice coefficient as a measure of overlap we demonstrated that the intra subject agreement was much higher than the inter subject agreement across all tracking algorithms and label sets. No significant differences were found for intra-subject comparisons. The inter-subject comparions indicate that the TEND method most consistently identifies similar subgraphs at a given density. However, further analysis of additional tracking parameters is necessary to determine the full set of conditions under which this result holds.

4.2 NETWORK SUMMARY MEASURES OVER GRAPH DENSITY

Global and local efficiency are the most robust to choice of fiber tracking algorithm, and have high levels of reproducibility across density levels. Assortativity and characteristic path length are highly reproducible across density levels, but are sensitive to choice of fiber tracking algorithm. In general, the portions of the graph curves at low density value and less reproducible than the segments at high density. For many metrics, the graph curves strongly converge at high density values suggesting that examining the metrics at those densities may be of little use. Examining both the mean graph curves and ICC plots may provide guidance for the range of densities that should be looked at in a group comparison study.

4.3 RICH CLUB COEFFICIENT OVER NODE-DEGREE

The examination of rich club coefficient as a function of degree-level demonstrates the use of graph curves over a parameter other than graph density. Consistency appears to have a somewhat inverse relationship to the coefficient as a function of node degree level. This is a result of the fact that the rich club coefficient values converge at high and low densities. Here, all graphs were thresholded at the maximum density achievable by all graphs. Because network size is held constant here, the average node degree would drop with lowered density, and additional work is required to more understand the relationship between graph-density and degree-level that would provide the most reproducible results.

4.4 LIMITATIONS AND FUTURE DIRECTIONS

The are a number of methodological limitations to the work presented here. We limited the fiber tracking to deterministic methods and used constant shared parameters for these methods. The influence of these parameters on individual tracking algorithms and the resulting graph metrics demands further exploration. In the choice of anatomical label sets, we limited the analysis to a set of manually defined labels, and a often used set of template-based labels. In each case we used the labels 'as-is' without upsampling to a higher number of regions. This may reduce the reproducibility of the networks, but provides more interpretable results if one wishes to examine individual connections or a subset of connections (e.g. default mode network) since the labels have well defined anatomical associations.

266 The use of a data with relatively low angular resolution and the use of the diffusion tensor model are
267 both limiting factors in the work presented here. To some degree, the choice of diffusion model is limited
268 by the data used here. However, these limitations are representative of a great deal of existing data sets.
269 Thus, the work presented here provides insight into the utility of using this data to examine network-
270 wide structural connectivity properties. Additionally this work provides a baseline analysis. This allows
271 methods using more sophisticated techniques, such as diffusion spectrum imaging and it's associated
272 models, to demonstrate the added value of those methods. Without this baseline, the added benefit of
273 these more complex techniques is less clear due to a lack of sufficient context.

274 An additional limitation of this work is the use of streamline count matrices as the basis for thresholding
275 to create constant density graphs. Multiple options exist for normalizing the streamline count matrices
276 using the volumes of the target cortical regions and/or the average length of the streamlines the connect
277 two regions. The volume based normalization may accomodate the differences that are seen between
278 graph curves that were generated using the different anatomical labels. However, the focus here was on
279 the influence of the fiber tracking and no direct comparisons were made between graph curves generated
280 from the different label sets. A number of additional options exist for creating a weighted connectivity
281 matrix including the average FA of fibers that connect two regions. Since the data set examined also
282 includes magnetization transfer data, the average magnetization transfer ratio along streamlines could
283 potentially be useful as it directly related to myelin content in white matter. These issues were beyond the
284 scope of the current study but would make for an intriguing extension of the current work.

285 The selection of graph metrics for analysis is another limitation of the study. An exhaustive examination
286 of all possible graph metrics was not feasible so metrics that have been studied previously were chosen
287 to give additional context to existing work. Many of the metrics examined have alternate formulations for
288 weighted graphs. Here, only unweighted graph metrics were examined as they are prevalent in current
289 literature. The creation of a testing framework that relies upon a public data set and open-source code was
290 intended to facilitate the further exploration of the issues listed here.

4.5 CONCLUSION

291 This study evaluate the reproducibility of graph summary metrics in structural brain networks derived
292 from DTI based deterministic fiber tractography. Four different fiber tracking algorithms were examined
293 along with two different anatomical label set. A number of graph metrics were examined by creating
294 graph curves that capture how a metric changes over a parameter such as graph density. ICC plots were
295 used to evaluate the reproducibility of the metrics and FDA was used to identify significant differences
296 between graph curves generated using different fiber tracking algorithms. While differences between the
297 tracking algorithms were not drastic, they were significant in many cases, suggesting that future studies
298 should give careful consideration to the choice of fiber tracking algorithm based upon the graph metric
299 that will be analyzed.

4.6 DATA SHARING

300 Free, publicly-available data and software was used throughout. The scripts used to generate the data
301 and figures are available at: <https://github.com/jeffduda/StructConnRepro>. This repos-
302 itory contains the configuration file that, when added to ITK, will download and compile Petiole which
303 builds the executables that were used to generate the graph metrics examined in this study. The tem-
304 plate with labels is available at [http://figshare.com/articles/Kirby_multivariate_](http://figshare.com/articles/Kirby_multivariate_template/852989)
305 [template/852989](http://figshare.com/articles/MMRR21_DTI_TTargets/850369), the final segmentations used as the target regions for fiber tracking are available at
306 http://figshare.com/articles/MMRR21_DTI_TTargets/850369 to provide a convenient
307 starting point for reproducing or extending the methods presented here.

DISCLOSURE/CONFLICT-OF-INTEREST STATEMENT

308 The authors declare that the research was conducted in the absence of any commercial or financial
309 relationships that could be construed as a potential conflict of interest.

REFERENCES

- 310 Basser, P. J., Pajevic, S., Pierpaoli, C., Duda, J., and Aldroubi, A. (2000) In vivo fiber tractography using
311 dt-mri data. *Magn Reson Med* 44 625–632.
- 312 Lazar, M., Weinstein, D. M., Tsuruda, J. S., Hasan, K. M., Arfanakis, K., Meyerand, M. E., et al.
313 (2003) White matter tractography using diffusion tensor deflection. *Hum Brain Mapp* 18 306–321.
314 doi:10.1002/hbm.10102.
- 315 Hagmann, P., Thiran, J.-P., Jonasson, L., Vanderghenst, P., Clarke, S., Maeder, P., et al. (2003) DtI
316 mapping of human brain connectivity: statistical fibre tracking and virtual dissection. *Neuroimage* 19
317 545–554.
- 318 Xue, R., van Zijl, P. C., Crain, B. J., Solaiyappan, M., and Mori, S. (1999) In vivo three-dimensional
319 reconstruction of rat brain axonal projections by diffusion tensor imaging. *Magn Reson Med* 42 1123–
320 1127.
- 321 Hagmann, P., Cammoun, L., Gigandet, X., Meuli, R., Honey, C. J., Wedeen, V. J., et al. (2008) Mapping
322 the structural core of human cerebral cortex. *PLoS Biol* 6 e159. doi:10.1371/journal.pbio.0060159.
- 323 Zalesky, A., Fornito, A., Harding, I. H., Cocchi, L., Yücel, M., Pantelis, C., et al. (2010) Whole-brain
324 anatomical networks: does the choice of nodes matter? *Neuroimage* 50 970.
- 325 Cheng, H., Wang, Y., Sheng, J., Sporns, O., Kronenberger, W. G., Mathews, V. P., et al. (2012a) Opti-
326 mization of seed density in dti tractography for structural networks. *J Neurosci Methods* 203 264–272.
327 doi:10.1016/j.jneumeth.2011.09.021.
- 328 Bastiani, M., Shah, N. J., Goebel, R., and Roebroek, A. (2012) Human cortical connectome reconstruc-
329 tion from diffusion weighted mri: the effect of tractography algorithm. *Neuroimage* 62 1732–1749.
330 doi:10.1016/j.neuroimage.2012.06.002.
- 331 Irimia, A. and Van Horn, J. D. (2012) The structural, connectomic and network covariance of the human
332 brain. *Neuroimage* 66C 489–499. doi:10.1016/j.neuroimage.2012.10.066.
- 333 Sporns, O. (2011) The non-random brain: efficiency, economy, and complex dynamics. *Front Comput
334 Neurosci* 5 5. doi:10.3389/fncom.2011.00005.
- 335 Fornito, A., Zalesky, A., Pantelis, C., and Bullmore, E. T. (2012) Schizophrenia, neuroimaging and
336 connectomics. *Neuroimage* 62 2296–2314. doi:10.1016/j.neuroimage.2011.12.090.
- 337 Xie, T. and He, Y. (2012) Mapping the alzheimer's brain with connectomics. *Frontiers in Psychiatry* 2.
338 doi:10.3389/fpsyg.2011.00077.
- 339 Guye, M., Bettus, G., Bartolomei, F., and Cozzone, P. J. (2010) Graph theoretical analysis of structural
340 and functional connectivity mri in normal and pathological brain networks. *MAGMA* 23 409–421.
341 doi:10.1007/s10334-010-0205-z.
- 342 Martin, G. (2012) Network analysis and the connectopathies: current research and future approaches.
343 *Nonlinear Dynamics Psychol Life Sci* 16 79–90.
- 344 Honey, C. J., Sporns, O., Cammoun, L., Gigandet, X., Thiran, J. P., Meuli, R., et al. (2009) Predicting
345 human resting-state functional connectivity from structural connectivity. *Proc Natl Acad Sci U S A* 106
346 2035–2040. doi:10.1073/pnas.0811168106.
- 347 Honey, C. J., Ktter, R., Breakspear, M., and Sporns, O. (2007) Network structure of cerebral cortex
348 shapes functional connectivity on multiple time scales. *Proc Natl Acad Sci U S A* 104 10240–10245.
349 doi:10.1073/pnas.0701519104.
- 350 Deuker, L., Bullmore, E. T., Smith, M., Christensen, S., Nathan, P. J., Rockstroh, B., et al. (2009)
351 Reproducibility of graph metrics of human brain functional networks. *Neuroimage* 47 1460–1468.
- 352 Telesford, Q. K., Morgan, A. R., Hayasaka, S., Simpson, S. L., Barret, W., Kraft, R. A., et al. (2010)
353 Reproducibility of graph metrics in fmri networks. *Frontiers in neuroinformatics* 4.
- 354 Braun, U., Plichta, M. M., Esslinger, C., Sauer, C., Haddad, L., Grimm, O., et al. (2012) Test-retest reli-
355 ability of resting-state connectivity network characteristics using fmri and graph theoretical measures.
356 *Neuroimage* 59 1404–1412.
- 357 Schwarz, A. J. and McGonigle, J. (2011) Negative edges and soft thresholding in complex network analy-
358 sis of resting state functional connectivity data. *Neuroimage* 55 1132–1146. doi:10.1016/j.neuroimage.
359 2010.12.047.

- 360 Liang, X., Wang, J., Yan, C., Shu, N., Xu, K., Gong, G., et al. (2012) Effects of different correlation
361 metrics and preprocessing factors on small-world brain functional networks: a resting-state functional
362 mri study. *PLoS one* 7 e32766.
- 363 Weber, M. J., Detre, J. A., Thompson-Schill, S. L., and Avants, B. B. (2013) Reproducibility of
364 functional network metrics and network structure: a comparison of task-related bold, resting asl
365 with bold contrast, and resting cerebral blood flow. *Cogn Affect Behav Neurosci* 13 627–640.
366 doi:10.3758/s13415-013-0181-7.
- 367 Cammoun, L., Gigandet, X., Meskaldji, D., Thiran, J. P., Sporns, O., Do, K. Q., et al. (2012) Mapping the
368 human connectome at multiple scales with diffusion spectrum mri. *J Neurosci Methods* 203 386–397.
369 doi:10.1016/j.jneumeth.2011.09.031.
- 370 Bassett, D. S., Brown, J. A., Deshpande, V., Carlson, J. M., and Grafton, S. T. (2011) Conserved and
371 variable architecture of human white matter connectivity. *Neuroimage* 54 1262–1279. doi:10.1016/j.
372 neuroimage.2010.09.006.
- 373 Dennis, E. L., Jahanshad, N., Toga, A. W., McMahon, K. L., de Zubicaray, G. I., Martin, N. G., et al.
374 (2012) Test-retest reliability of graph theory measures of structural brain connectivity. *Med Image
375 Comput Comput Assist Interv* 15 305–312.
- 376 Owen, J. P., Ziv, E., Bukshpun, P., Pojman, N., Wakahiro, M., Berman, J. I., et al. (2013) Test-retest reli-
377 ability of computational network measurements derived from the structural connectome of the human
378 brain. *Brain Connect* 3 160–176. doi:10.1089/brain.2012.0121.
- 379 Vaessen, M. J., Hofman, P. A. M., Tijssen, H. N., Aldenkamp, A. P., Jansen, J. F. A., and Backes,
380 W. H. (2010) The effect and reproducibility of different clinical dti gradient sets on small world brain
381 connectivity measures. *Neuroimage* 51 1106–1116. doi:10.1016/j.neuroimage.2010.03.011.
- 382 Cheng, H., Wang, Y., Sheng, J., Kronenberger, W. G., Mathews, V. P., Hummer, T. A., et al. (2012b) Char-
383 acteristics and variability of structural networks derived from diffusion tensor imaging. *Neuroimage* 61
384 1153–1164. doi:10.1016/j.neuroimage.2012.03.036.
- 385 Telesford, Q. K., Burdette, J. H., and Laurienti, P. J. (2013) An exploration of graph metric reproducibility
386 in complex brain networks. *Front Neurosci* 7 67. doi:10.3389/fnins.2013.00067.
- 387 Klein, A. and Tourville, J. (2012) 101 labeled brain images and a consistent human cortical labeling
388 protocol. *Front Neurosci* 6 171. doi:10.3389/fnins.2012.00171.
- 389 Tzourio-Mazoyer, N., Landeau, B., Papathanassiou, D., Crivello, F., Etard, O., Delcroix, N., et al. (2002)
390 Automated anatomical labeling of activations in spm using a macroscopic anatomical parcellation of
391 the mni mri single-subject brain. *Neuroimage* 15 273–289. doi:10.1006/nimg.2001.0978.
- 392 Landman, B. A., Huang, A. J., Gifford, A., Vikram, D. S., Lim, I. A. L., Farrell, J. A. D., et al. (2011)
393 Multi-parametric neuroimaging reproducibility: a 3-t resource study. *Neuroimage* 54 2854–2866. doi:
394 10.1016/j.neuroimage.2010.11.047.
- 395 Avants, B. B., Tustison, N., and Song, G. (2009) Advanced normalization tools (ants). *Insight J.*
396 Tustison, N. J., Avants, B. B., Cook, P. A., Zheng, Y., Egan, A., Yushkevich, P. A., et al. (2010)
397 N4itk: improved n3 bias correction. *IEEE Trans Med Imaging* 29 1310–1320. doi:10.1109/TMI.
398 2010.2046908.
- 399 Cook, P., Bai, Y., Nedjati-Gilani, S., Seunarine, K., Hall, M., Parker, G., et al., Camino: Open-source
400 diffusion-mri reconstruction and processing. *14th scientific meeting of the international society for
401 magnetic resonance in medicine* (2006), volume 2759.
- 402 Basser, P. J., Mattiello, J., and LeBihan, D. (1994) Estimation of the effective self-diffusion tensor from
403 the nmr spin echo. *J Magn Reson B* 103 247–254.
- 404 Salvador, R., Pea, A., Menon, D. K., Carpenter, T. A., Pickard, J. D., and Bullmore, E. T. (2005) Formal
405 characterization and extension of the linearized diffusion tensor model. *Hum Brain Mapp* 24 144–155.
406 doi:10.1002/hbm.20076.
- 407 Achard, S., Salvador, R., Whitcher, B., Suckling, J., and Bullmore, E. (2006) A resilient, low-frequency,
408 small-world human brain functional network with highly connected association cortical hubs. *The
409 Journal of Neuroscience* 26 63–72.
- 410 Bassett, D. S., Meyer-Lindenberg, A., Achard, S., Duke, T., and Bullmore, E. (2006) Adaptive reconfig-
411 uration of fractal small-world human brain functional networks. *Proceedings of the National Academy
412 of Sciences* 103 19518–19523.

- 413 Rubinov, M. and Sporns, O. (2010) Complex network measures of brain connectivity: uses and
414 interpretations. *Neuroimage* 52 1059–1069. doi:10.1016/j.neuroimage.2009.10.003.
- 415 Newman, M. E. J. (2006) Modularity and community structure in networks. *Proc Natl Acad Sci U S A*
416 103 8577–8582. doi:10.1073/pnas.0601602103.
- 417 Bassett, D. S., Bullmore, E., Verchinski, B. A., Mattay, V. S., Weinberger, D. R., and Meyer-Lindenberg,
418 A. (2008) Hierarchical organization of human cortical networks in health and schizophrenia. *J Neurosci*
419 28 9239–9248. doi:10.1523/JNEUROSCI.1929-08.2008.
- 420 Watts, D. J. and Strogatz, S. H. (1998) Collective dynamics of 'small-world' networks. *Nature* 393
421 440–442. doi:10.1038/30918.
- 422 Latora, V. and Marchiori, M. (2001) Efficient behavior of small-world networks. *Physical review letters*
423 87 198701.
- 424 Collin, G., Sporns, O., Mandl, R. C., and van den Heuvel, M. P. (2013) Structural and functional aspects
425 relating to cost and benefit of rich club organization in the human cerebral cortex. *Cerebral Cortex*.
- 426 Tustison, N., Yushkevich, P., Song, Z., and Gee, J. (2008) Graph cuts, caveat utilitor, and euler's bridges
427 of konigsberg. *Insight Journal* July <http://hdl.handle.net/1926/1503>.
- 428 Newman, M. E. (2002) Assortative mixing in networks. *Physical review letters* 89 208701.
- 429 Dijkstra, E. W. (1959) A note on two problems in connexion with graphs. *Numerische mathematik* 1
430 269–271.
- 431 Colizza, V., Flammini, A., Serrano, M. A., and Vespignani, A. (2006) Detecting rich-club ordering in
432 complex networks. *Nature physics* 2 110–115.
- 433 Montgomery, A. A., Graham, A., Evans, P. H., and Fahey, T. (2002) Inter-rater agreement in the scoring
434 of abstracts submitted to a primary care research conference. *BMC Health Services Research* 2 8.